

Effects of the Hubbard U on density functional-based predictions of BiFeO₃ properties

This content has been downloaded from IOPscience. Please scroll down to see the full text.

Download details:

IP Address: 128.41.35.98

This content was downloaded on 06/09/2017 at 12:33

Manuscript version: Accepted Manuscript

Shenton et al

To cite this article before publication: Shenton et al, 2017, J. Phys.: Condens. Matter, at press:

<https://doi.org/10.1088/1361-648X/aa8935>

This Accepted Manuscript is: © 2017 IOP Publishing Ltd

During the embargo period (the 12 month period from the publication of the Version of Record of this article), the Accepted Manuscript is fully protected by copyright and cannot be reused or reposted elsewhere.

As the Version of Record of this article is going to be / has been published on a subscription basis, this Accepted Manuscript is available for reuse under a CC BY-NC-ND 3.0 licence after the 12 month embargo period.

After the embargo period, everyone is permitted to copy and redistribute this article for non-commercial purposes only, provided that they adhere to all the terms of the licence

<https://creativecommons.org/licences/by-nc-nd/3.0>

Although reasonable endeavours have been taken to obtain all necessary permissions from third parties to include their copyrighted content within this article, their full citation and copyright line may not be present in this Accepted Manuscript version. Before using any content from this article, please refer to the Version of Record on IOPscience once published for full citation and copyright details, as permission will likely be required. All third party content is fully copyright protected, unless specifically stated otherwise in the figure caption in the Version of Record.

When available, you can view the Version of Record for this article at:

<http://iopscience.iop.org/article/10.1088/1361-648X/aa8935>

Effects of the Hubbard U on density functional-based predictions of BiFeO₃ properties

J. Kane Shenton^{1,2,3}, David R. Bowler^{1,3,4}, Wei Li Cheah²

E-mail: john.shenton.10@ucl.ac.uk

¹ Department of Physics & Astronomy, University College London, Gower St, London, WC1E 6BT

² Institute of High Performance Computing, 1 Fusionopolis Way, #16-16 Connexis North, Singapore 138632

³ London Centre for Nanotechnology, 17-19 Gordon St, London, WC1H 0AH

⁴ International Centre for Materials Nanoarchitectonics (WPI-MANA), National Institute for Materials Science (NIMS), 1-1 Namiki, Tsukuba, Ibaraki 305-0044, Japan

Abstract.

First principles studies of multiferroic materials, such as bismuth ferrite (BFO), require methods that extend beyond standard density functional theory (DFT). The DFT+U method is one such extension that is widely used in the study of BFO. We present a systematic study of the effects of the U parameter on the structural, ferroelectric and electronic properties of BFO. We find that the structural and ferroelectric properties change negligibly in the range of U typically considered for BFO (3–5 eV). In contrast, the electronic structure varies significantly with U. In particular, we see large changes to the character and curvature of the valence band maximum and conduction band minimum, in addition to the expected increase in band gap, as U increases. Most significantly, we find that the t_{2g}/e_g ordering at the conduction band minimum inverts for U values larger than 4 eV. We therefore recommend a U value of at most 4 eV to be applied to the Fe d orbitals in BFO. More generally, this study emphasises the need for systematic investigations of the effects of the U parameter not merely on band gaps but on the electronic structure as a whole, especially for strongly correlated materials.

Submitted to: *J. Phys.: Condens. Matter*

1. Introduction

The magnetoelectric multiferroic material, bismuth ferrite (BiFeO_3 ; BFO), combines a spontaneous polarisation with an antiferromagnetic ordering in a single phase, at room temperature. This combination of properties makes BFO an interesting material for both fundamental research and a wide range of applications, from spintronics [1] to photovoltaics [2, 3]. In photovoltaic applications, the giant spontaneous polarisation ($\sim 100 \mu\text{C}/\text{cm}^2$ [4, 5]) is thought to aid in charge separation via the bulk photovoltaic effect [6, 7]. Ferroelectric (FE) domains are thought to further enhance the photovoltaic prospects of BFO by allowing above-band gap photovoltages across the FE domains [8], and conduction along them [9].

Another attractive feature of the BFO system is the tunability of its properties with experimentally accessible changes to its crystal structure. A wide range of crystal structures with widely varying optoelectronic properties can be stabilised through the epitaxial strain engineering of BFO thin films [10, 11]. The subtle interplay between structural and electronic degrees of freedom that underlies the tunability of the BFO system, however, make this material particularly challenging to model. For example, the weak (Dzyaloshinskii-Moriya) ferromagnetism observed in BFO cannot be captured without including the effects of spin-orbit coupling (SOC) [12].

More generally, standard density functional theory (DFT) methods are known to have systematic failures in describing the electronic structure of materials with strongly correlated d states, such as BFO. In particular, standard local density and generalised gradient approximations of the exchange-correlation (xc) functional incorrectly describe the on-site Coulomb interactions of highly localised electrons, due to erroneous electron self-interaction. This failure to describe strongly localised states exacerbates the infamous band gap problem in DFT.

A number of techniques can be used to improve the description of localised electronic states, such as self-interaction correction methods and the use of hybrid functionals. While hybrid functionals, in particular the Heyd-Scuseria-Ernzerhof (HSE) screened hybrid functional, have been shown to accurately capture many properties of BFO, they come at a vastly increased ($\sim 50\times$) computational cost compared to standard DFT [13]. For simple bulk BFO, the additional cost is perfectly feasible on modern computer architectures. However, exciting developments in the study of BFO suggest that ferroelectric domains [1, 14, 9], doping [15, 16] and hetero-interfaces [17, 18, 19, 20, 21] with this material hold great technological promise. The theoretical investigation of such systems requires large simulation cells, which can be prohibitively expensive using hybrid functionals.

One of the most computationally cost-effective corrections to standard DFT is the ‘DFT+U’ method. In this method an on-site Hubbard-like correction is applied to the effective potential. Two free parameters, U and J , can be used to effectively tune the on-site Coulomb and exchange interactions respectively. In the approach of Dudarev *et al.* [22], these are replaced by a single parameter, $U_{\text{eff}} = U - J$. While the U_{eff}

parameter can be obtained from *ab initio* calculations [23], it is typically chosen semi-empirically by comparing some predicted property to the available experimental data. The property used for calibration purposes depends on the intended aim of the study, with the electronic band gap and oxidation energies [24] being two of the most commonly chosen.

Careful tests are required, however, to ensure that other material properties are not adversely affected by one's choice of U_{eff} . For example, if U_{eff} is chosen such that the predicted band gap agrees with experiment, one should ensure that no significant error is introduced into the calculated lattice parameter as a result. Previous studies of the effects of the U_{eff} parameter have been conducted on the structural and electronic properties of BFO. Neaton *et al.* found that choosing a value of $U_{\text{eff}} = 4$ eV within the local spin density approximation (i.e. the LDA+U) improves the accuracy of the calculated lattice parameter, rhombohedral cell angle and the electronic band gap [25]. For their finite-temperature study of BFO, Kornev *et al.* used the scheme of Cococcioni and de Gironcoli [26] to self-consistently determine the value of U within the LDA+U to be 3.8 eV [27]. However, they found that the parameters in their effective Hamiltonian were extremely sensitive to the value of U , stating that some of these parameters changed by about 20% when U was slightly reduced from 3.8 to 3.5 eV. Applying the U correction to the generalised gradient approximation (GGA+U), a U value of 5 eV was determined by Young *et al.* to most accurately reproduce the experimental imaginary permittivity near the band gap [28].

The effects of the U_{eff} parameter on the crystal structure, band gap and permittivity of BFO are therefore known, but those on other electronic properties have not yet been reported for BFO as far as we are aware. In this paper we extend the systematic study of the U_{eff} parameter to include the curvature and character of the band edges in BFO. We find that the electron and hole effective masses, inversely proportional to the band curvature, are highly sensitive to the chosen value of U_{eff} and that the ordering of the Fe d orbitals at the conduction band minimum inverts for $U_{\text{eff}} > 4$ eV. These findings have important implications for theoretical studies of BFO and related materials, especially in cases where the charge carrier effective masses and band character play significant roles, such as in photovoltaics [29].

2. Methods

All of the results presented here are based on DFT simulations using version 5.4.1 of the Vienna *ab initio* Simulation Package [30, 31, 32, 33] (VASP). The calculations were carried out using the projector-augmented plane-wave method [34, 35], treating explicitly 15 electrons for Bi ($5d^{10}6s^26p^3$), 14 for Fe ($3p^63d^64s^2$), and 6 for O ($2s^22p^4$). ‡ We use a plane-wave cut-off energy of 520 eV and perform Brillouin zone integrations on a Γ -centred $9 \times 9 \times 9$ Monkhorst-Pack mesh [36]. The GGA xc functional parameterised by Perdew, Burke and Ernzerhof (PBE) [37] is used throughout the paper, with

‡ The Bi, Fe and O PAWs are dated: 6th Sept. 2000, 2nd Aug. 2007 and 8th Apr. 2002 respectively

1
2
3
4
5
6
7
8
9
10
11
12
13
14
15
16
17
18
19
20
21
22
23
24
25
26
27
28
29
30
31
32
33
34
35
36
37
38
39
40
41
42
43
44
45
46
47
48
49
50
51
52
53
54
55
56
57
58
59
60

comparisons to the LDA and PBEsol [38] functionals where appropriate. We apply the effective Hubbard-like correction, U_{eff} , to the Fe d orbitals using the method of Dudarev *et al.* [22], varying the magnitude of U_{eff} between 0 and 8 eV.

We use the ground-state, rhombohedral BFO structure (spacegroup: $R\bar{3}c$) [39] as our model for all calculations. This phase exhibits a large spontaneous polarisation along the pseudo-cubic [111] direction ($[111]_{pc}$), primarily due to a Bi translation along this direction. This phase adopts a nearly G-type antiferromagnetic ordering [40] which we approximate as exactly G-type by using a 10-atom unit cell (two formula units), with the spin on the Fe atoms alternating along the $[111]_{pc}$ direction. See the insets in Fig. 2 for a depiction of the structure used.

As previously mentioned, SOC has been found to be significant in describing the weak ferromagnetism in BFO [12]. However, SOC has been found to negligibly affect the curvature and character of the band edges in $R\bar{3}c$ BFO [29]. In particular, for the $U_{\text{eff}} = 4$ eV relaxed structure, the calculated absolute hole effective mass increased from $0.748 m_0$ with SOC to $0.763 m_0$ without SOC, where m_0 is the electron rest mass. Similarly, the electron effective mass increased from $2.950 m_0$ with SOC, to $3.017 m_0$ without SOC. Such differences are significantly smaller than those being investigated here, and we therefore neglect SOC hereafter.

The following procedure was repeated for each value of U_{eff} , tested in the range $0 \leq U_{\text{eff}} \leq 8$ eV: first, a full geometry optimisation was performed in which the internal coordinates were relaxed such that all force components were less than $2 \text{ meV}/\text{\AA}$. The unit cell shape and size were optimised such that all stress components were smaller than 2 MPa . Following the geometry optimisation, an accurate self-consistent calculation was performed.

The spontaneous polarisation, P_s , was calculated using the Modern Theory of Polarisation (MTP) [41, 42, 43]. We note that, according to the MTP, only *differences* in polarisation are well-defined, and that bulk polarisation is best understood as a lattice of values [41, 42, 43]. In general, one needs to construct a ferroelectric switching path to resolve the ambiguity in the calculated polarisation - i.e. to find out on which branch of the polarisation lattice the calculated polarisation lies. By constructing such a switching path, we found that P_s is related to our raw calculated polarisation, P_{calc} , and the so-called quantum of polarisation, Q , via $P_s = P_{\text{calc}} + Q/2$. For more details on the necessity of this additional step in the context of BFO, see Ref. [25].

To calculate the charge carrier effective mass, m^* , we require the second derivative of the dispersion relation for a given band and location in reciprocal space. In general, effective masses are anisotropic and so a full effective mass tensor is required. We obtain the full effective mass tensors at the valence band maximum (VB_{max}) and conduction band minimum (CB_{min}) following the procedure outlined in Ref. [29], using the method and code found in Ref. [44]. Briefly, the method involves generating a fine mesh around the k -point of interest, calculating the energy eigenvalues at fixed, self-consistent charge density, and using a finite difference method to build up the tensor of second derivatives. The dependence of m^* on the mesh spacing parameter was investigated and spacings

of less than 0.05 bohr^{-1} were found to give consistent results [29]. In order to compare the effective masses at different values of U_{eff} we calculated the eigenvalues of each m^* tensor, which correspond to the m^* along the principle directions, and selected the smallest eigenvalue in each case.

Several alternative approaches to estimating m^* exist. One could, for example, focus on the curvature of a fixed band at a fixed k -point, for all values of U_{eff} . This has the benefits of being more straightforward, and of isolating changes in the curvature of the chosen band from changes to the location and character of the band edges. Another approach would be to average m^* across the whole of the lowest band or set of bands as was done by Hautier *et al.* [45, 46]. The latter approach is of particular value in cases where the bands around the Fermi level are very flat, since in such cases multiple band extrema become energetically relevant to conduction. In this work we choose to focus on the curvature of VB_{max} and CB_{min} , although the location may change with U_{eff} , in order to emphasise the role of these points in determining the response of the conduction electrons/holes. With this approach, we find that abrupt changes in m^* provides an indication of changes to the character of the band edges.

Finally, we computed the electronic density of states. We note that, because the FeO_6 octahedra do not align with the Cartesian axes in the rhombohedral unit-cell setting, VASP fails to correctly model the fine details of the projected DOS. In particular, in the rhombohedral setting, the DOS does not exhibit any of the typical splitting of the Fe d orbitals that one would expect given the octahedral environment of Fe. To obtain more detailed and accurate DOS projections we converted each of the relaxed structures into their 40-atom, pseudo-cubic, unit cell setting. Although the FeO_6 octahedral axes still do not line up perfectly with the Cartesian axes in this setting (due to the tilting of the octahedra), a clear splitting between the projected t_{2g} and e_g states is observed in this setting, as expected by symmetry. To obtain a more accurate DOS, a finer $11 \times 11 \times 11$ Monkhorst-Pack mesh was used, in addition to using the larger 40-atom unit cell.

The full VASP input files and structures are available at Ref. [47].

3. Results and Discussion

3.1. Crystal structure

In Fig. 1 we plot the relaxed rhombohedral lattice parameter and angle as we vary U_{eff} in the PBE+U xc functional. We compare the response of the PBE+U functional to that of two other commonly used xc functionals: PBEsol+U and LDA+U functionals. We find that, for all three xc functionals, increasing U_{eff} up to 4 eV leads to an increase in lattice parameter and a decrease in rhombohedral angle, in agreement with Neaton *et al.* [25]. We note that an increase in lattice parameter with U_{eff} represents an improvement in structural accuracy for the LDA+U because of its tendency to overbind. In contrast, because the PBE functional underbinds BFO, an increase in

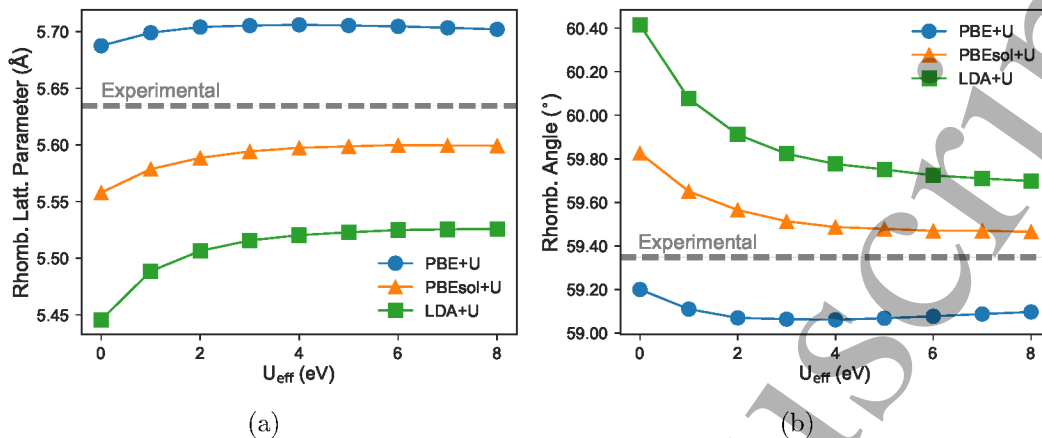


Figure 1. Rhombohedral (a) lattice parameters and (b) cell angles as a function of U_{eff} across the PBE+U (blue circles), PBEsol+U (orange triangles) and LDA+U (green squares) xc functionals. The dotted ‘experimental’ line in each comes from the (298 K) structure provided in Ref. [39]. The reported uncertainty of the experimental values is too small to be seen on this scale.

lattice parameter constitutes a decrease in accuracy. Nevertheless, even the least accurate lattice parameter found with PBE+U ($< 1.3\%$ error, occurring when $U_{\text{eff}} = 4$ eV) is in better agreement with the experimental lattice parameter of $5.63443(5)$ Å [39], than the most accurate LDA+U value ($> 1.9\%$ error, occurring when $U_{\text{eff}} = 8$ eV). Interestingly, the PBEsol+U slightly overbinds BFO for all value of U , though performs significantly better than both the LDA+U and the PBE+U, with a lattice parameter error of 0.6% occurring when $U_{\text{eff}} = 5-8$ eV.

The error in lattice parameter can be further reduced to $\approx 0.3\%$ by using the hybrid HSE functional, as reported by Stroppa *et al.* [13]. However, while very accurately reproducing the experimental lattice parameter, the authors note that this method requires around 50 times more computational time per self-consistent step than does plain PBE or PBE+U. The HSE method is therefore limited to small unit cells. For larger cells, such as those required to model defects, grain boundaries or domains, the more computationally cost-effective PBE+U method may be preferred. Stroppa *et al.* also report a PBE relaxed structure with which our PBE results is in near perfect agreement: our calculated lattice parameter for $U_{\text{eff}} = 0$ eV, 5.687 Å, agrees exactly (to all reported digits) with their results, and the rhombohedral angle differs by just 0.02° .

Interestingly, for U_{eff} larger than 4 eV, we see the trend in lattice parameter and rhombohedral angle reverse. This effect may be driven by the qualitative change in the electronic structure that occurs around $U_{\text{eff}} = 4$ eV (as discussed in section 3.3). However, further work would be needed to establish this link.

In addition to the changes in the unit cell parameters, we observe changes in the internal coordinates of the atoms, as U_{eff} is increased. We are particularly interested in the two key structural transformations in $R3c$ BFO relative to the cubic perovskite structure. The first is a translation of the Bi ions *along* the $[111]_{pc}$ direction; the second

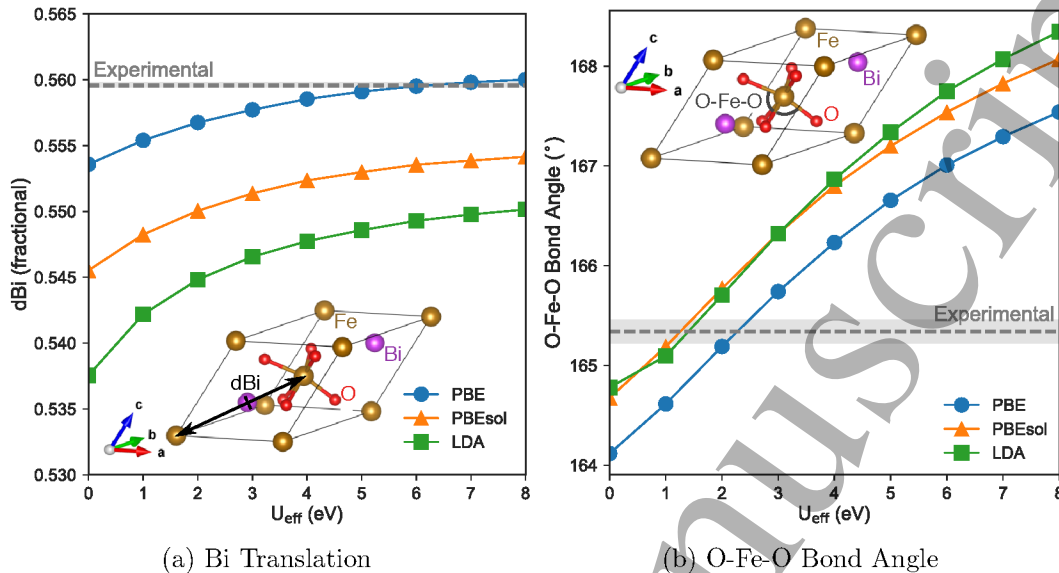


Figure 2. Effects of U_{eff} on (a) position of Bi along the $[111]_{pc}$ direction as a fraction of Fe-Fe separation, and (b) O-Fe-O bond angle. Results from PBE+ U (blue circles), PBEsol+ U (orange triangles) and LDA+ U (green squares) xc functionals are shown. The dotted ‘experimental’ line in each is measured from the (298 K) structure provided in Ref. [39], and the shaded range represents the uncertainty of those measurements. Note that in (a) this uncertainty is too small to be visible. The inset figures in each panel represent the $R3c$ structure and indicate the quantity being measured.

is an out-of-phase rotation of the FeO_6 octahedra *about* the $[111]_{pc}$ direction ($a^-a^-a^-$ in the notation of Glazer [48]). The former is the main driver for the large spontaneous polarisation in BFO, while the latter is thought to influence properties of BFO such as the charge carrier effective masses [29], polar order [18, 21] and spin state [49].

In Fig. 2a, we represent the translation of Bi by plotting its position as a fraction of Fe-Fe separation along the $[111]_{pc}$ direction. In the perfect cubic perovskite structure, a Bi atom would lie exactly halfway between two Fe atoms in the $[111]_{pc}$ direction (i.e. $d\text{Bi} = 0.5$ as defined in Fig. 2a). Compared with the experimental fractional translation, $d\text{Bi}_{\text{exp}} = 0.55958(18)$, we see an improvement in the description of the translation of Bi as U_{eff} is increased. At $U_{\text{eff}} = 6$ eV, $d\text{Bi}$ most closely matches that found in experiment. Note that we compare the fractional displacement of Bi (as opposed to absolute displacements), in order to take into account the changing lattice parameters at each value of U_{eff} .

In the $R3c$ structure of BFO, the FeO_6 octahedra are rotated about $[111]_{pc}$ by $\sim 14^\circ$. We find that the angle of rotation changes by $\approx 0.4^\circ$ when varying U_{eff} between 0 and 8 eV. Given that the angle of this rotation found in experiment spans the range $11\text{--}14^\circ$ [50, 51, 52], we conclude that the change in octahedral rotation due to U_{eff} is negligible.

Another manifestation of the distortion of $R3c$ BFO with respect to the cubic perovskite structure is the deviation of the O-Fe-O octahedral angle from 180° . We find

that the dependence of this angle on U_{eff} is also small, increasing from 164.1° to 167.5° as U_{eff} increases from 0 to 8 eV. In Fig. 2b we show this increase in O-Fe-O bond angle towards 180° as a function of U_{eff} . Nevertheless, all of the O-Fe-O angles predicted here are in reasonably good agreement with the experimental angle of $165.34(12)^\circ$, determined by high-resolution neutron diffraction at 298 K [39].

3.2. Polarisation

From the observed changes to the lattice geometry with varying U_{eff} , one might expect the spontaneous polarisation P_s to be affected. The increased Bi translation with U_{eff} would suggest an *increase* in P_s with increasing U_{eff} since the dipole moment per unit cell increases. However, as we have found the lattice parameter (and hence unit cell volume) increases with U_{eff} , we may expect an overall *decrease* in P_s as U_{eff} increases (recall that polarisation is inversely proportional to unit cell volume). We note that the structural changes due to U_{eff} may affect both the ionic and the electronic contributions to P_s . At the same time, independent of any structural changes, increasing U_{eff} itself may result in additional changes to the electronic contribution. We distinguish between structural and purely electronic effects by calculating P_s both for the DFT relaxed structures ('relaxed'), and for a chosen fixed structure ('fixed') in which we only vary U_{eff} . The fixed structure used for this purpose was that relaxed at $U_{\text{eff}} = 4$ eV.

In Fig. 3 we plot the variation in P_s with increasing U_{eff} for both the relaxed and fixed set of structures. There are two regimes present in Fig. 3: a sharp decrease in P_s with respect to U_{eff} , followed by much weaker dependence. The first regime, $U_{\text{eff}} \leq 2$ eV, can be explained by the sharp increase in lattice parameters. We note that the increase in lattice parameters dominates over the increase in Bi translation along $[111]_{pc}$ that would otherwise suggest an *increase* in P_s . The second regime, $U_{\text{eff}} > 2$ eV, in which we see a weaker dependence of P_s on U_{eff} , is dominated by changes only in the electronic structure, as the relaxed and fixed structure cases have the same dependence on U_{eff} beyond 2 eV.

As with the changes in lattice parameter and angles with U_{eff} , the most significant change in P_s occurs between a U_{eff} of 0 and 2 eV, with only minor changes thereafter. Since the typical values of U_{eff} chosen for Fe d orbitals in BFO lie between 3 and 5 eV [25, 27, 53, 54, 28, 55, 15, 56, 16], the accuracy of calculated unit cell parameters and P_s depends more on the choice to use the PBE+U method at all, rather than on the particular value of U_{eff} one chooses. Thus, within the range of U_{eff} usually considered in the context of BFO, we conclude that the crystal structure varies negligibly with U_{eff} .

3.3. Electronic structure

The influence of U_{eff} on the band character and curvature, often neglected in studies using DFT+U, will be the focus of this section. We quantify the curvature at the band extrema by calculating the charge carrier effective masses (Fig. 4), and represent the character using projected band structures and DOS (Fig. 5).

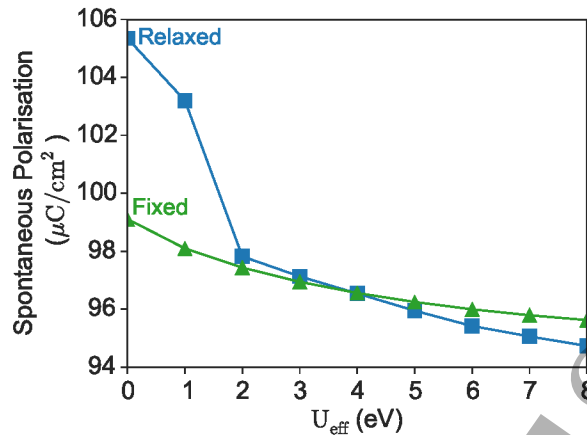


Figure 3. Variation in calculated spontaneous polarisation as a function of U_{eff} . We compare two cases: one in which we relax the structure fully for each value of U_{eff} (blue squares), and the second, in which we keep the structure fixed (green triangles) to that of $U_{\text{eff}} = 4$ eV.

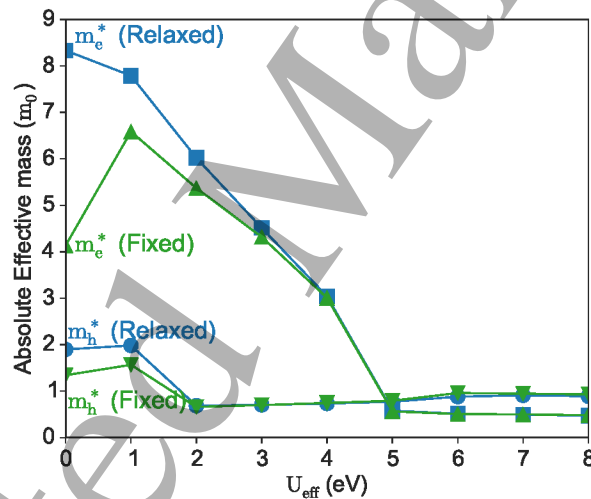


Figure 4. Absolute charge carrier effective mass versus U_{eff} . Blue squares and circles respectively represent the electron and hole effective masses for the DFT relaxed structures. Green triangles pointing up and down represent, respectively, the electron and hole effective masses for the fixed structure (fixed to the $U_{\text{eff}} = 4$ eV structure). m_e^* and m_h^* are the electron and hole effective masses, in units of the electron rest mass, m_0^* .

As with the polarisation, changes to the effective masses with U_{eff} can be broken down into structural contributions (by relaxing the structure at each U_{eff}) and purely electronic ones (by keeping the structure fixed in each case). In Fig. 4 we plot the electron and hole effective masses as a function of U_{eff} for both the relaxed and fixed structures.

For the relaxed structures we see a large reduction in the electron effective mass m_e^* : from $8.3 m_0$ for $U_{\text{eff}} = 0$ eV to $0.6 m_0$ for $U_{\text{eff}} = 5$ eV, indicating an increase in curvature at the CB_{min} with increasing U_{eff} . Between a U_{eff} of 5 and 8 eV we see little

($\sim 0.1 m_0$) further change in m_e^* . The curvature of the VB_{\max} also increases with U_{eff} , though most of the change occurs between a U_{eff} of 0 and 2 eV. The hole effective mass m_h^* decreases from $1.9 m_0$ for $U_{\text{eff}} = 0$ eV to $0.7 m_0$ for $U_{\text{eff}} = 2$ eV.

For the cases in which the structure was kept fixed to the $U_{\text{eff}} = 4$ eV relaxed structure, we see a similar dependence of m^* on U_{eff} . This similarity in trend between the relaxed and fixed structure cases indicates that changes in m_h^* and m_e^* with U_{eff} are dominated by changes purely to the electronic structure. The notable exception to this similarity is the m_e^* calculated for the fixed structure when $U_{\text{eff}} = 0$ eV ($m_e^* = 4.1 m_0$). The reason for this anomaly is a change in the location of the CB_{\min} relative to all other $U_{\text{eff}} < 5$ eV cases. The CB_{\min} for the anomalous result lies between Γ and $Z = [\frac{1}{2}, \frac{1}{2}, \frac{1}{2}]$, rather than exactly at Z as it is for the other $U_{\text{eff}} < 5$ eV cases. We attribute the change in location to the effective tensile strain resulting from using the $U_{\text{eff}} = 4$ eV relaxed geometry; see Ref. [29] for more details on the effects of strain on m^* in BFO.

In order to explain the observed changes in m^* with U_{eff} , we investigate changes to the band character as U_{eff} increases. We represent the band character using the projected band structure shown in Fig. 5. The contributions from O, Fe and Bi to each band at each k -point are represented on a normalised colourspace by red, green and blue respectively. Similar figures comparing the projected bands of the PBE+U, PBEsol+U and LDA+U xc functionals can be found in Fig. S6 of the SI [47]. We find only minor differences between the band structures of these three xc functionals. We also present the projected density of states (DOS) in this figure, in order to resolve the contributions from individual orbitals.

Beginning with the character of the valence bands, we make the following observations. A change in the character of the topmost valence bands, occurring between a U_{eff} of 0 and 2 eV, is clear from the colour change in the bands. The change from a mix of red and green at $U_{\text{eff}} = 0$ eV to almost pure red at $U_{\text{eff}} = 2$ eV in the topmost valence band (VB) indicates a reduction in the Fe-O hybridisation, leaving O to dominate the VB_{\max} . From the projected DOS we resolve these contributions further: at $U_{\text{eff}} = 0$ eV, the top of the VB is made up of a hybridisation of O p and Fe e_g states; the character of these bands changes to primarily O p , with minor contributions from Bi s and Fe e_g states above a U_{eff} of about 2 eV. The change in the character corresponds to the decrease in m_h^* at $U_{\text{eff}} = 2$ eV. Given that the lattice vectors change most significantly in the 0 to 2 eV range of U_{eff} , we might expect that the changes to the crystal structure of BFO are driving this shift in band character. However, as we saw in Fig. 4, the associated pattern in m_h^* is similar in both the relaxed and fixed structure cases, indicating that the change is dominated by purely electronic effects. That this is not purely a structural effect is confirmed by observing the same shift in character in the projected bands and DOS for the fixed structure calculations, which can be found in Fig. S4 [47].

In addition to the decrease in Fe contributions to the VB_{\max} , the projected DOS shows that a Bi s antibonding peak moves up in energy from around 1.5 eV below the VB_{\max} for U_{eff} of 0 eV, to the VB_{\max} itself for $U_{\text{eff}} \geq 2$ eV. The presence of a small Bi s contribution to the VB_{\max} is consistent with the HSE hybrid functional results by

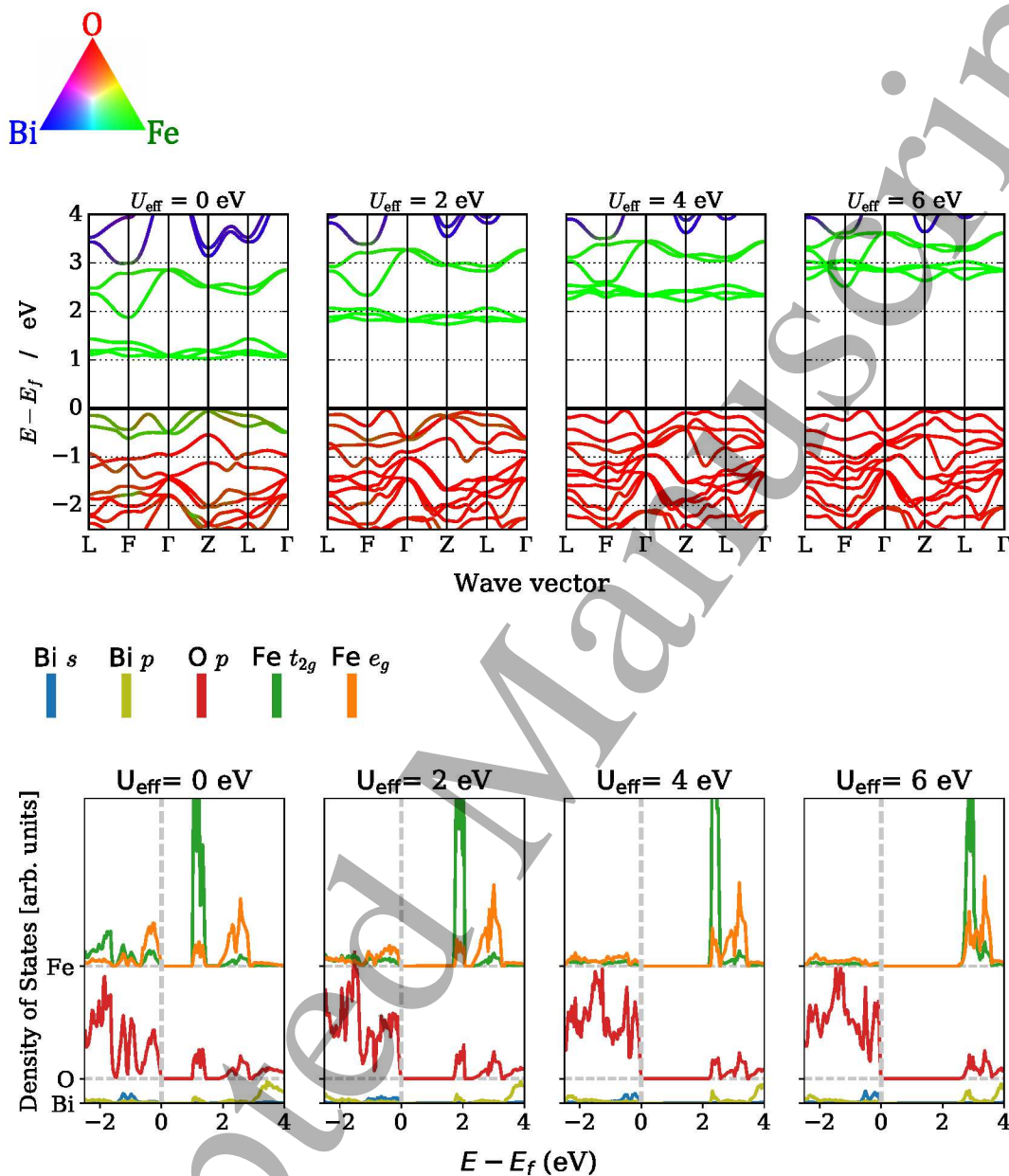


Figure 5. Variation in projected bands (top row) and density of states (bottom row) as a function of U_{eff} . The bands are coloured, at each k -point, based on wavefunction projections onto the elements. The contributions from O, Fe and Bi are represented on a normalised colourspace by red, green and blue respectively as shown by the colour triangle. The DOS is calculated in the pseudo-cubic setting in order to obtain accurate projections onto the selected atomic orbitals (indicated by the coloured vertical lines). Note that, since BFO adopts a G-type anti-ferromagnetic ordering, the spin up and spin down contributions are symmetrical. Here we are plotting the sum over both spin channels and over all atoms of each species.

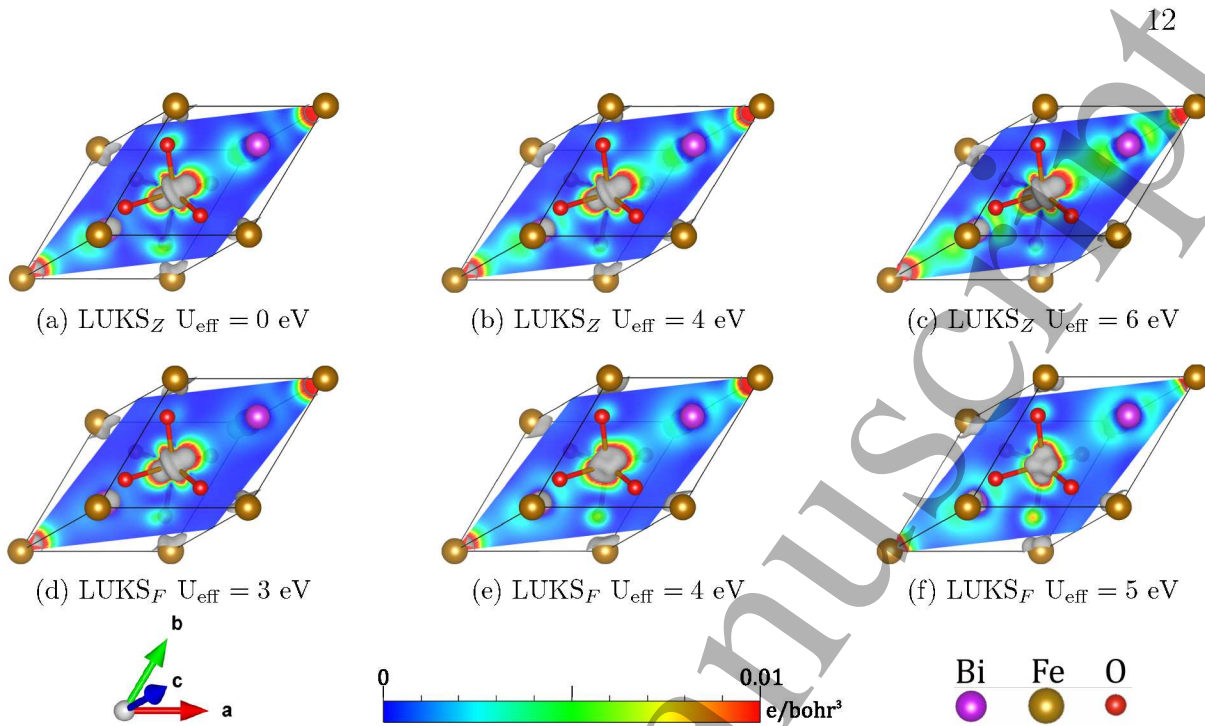


Figure 6. Lowest unoccupied KS orbitals (LUKS) at the Z (a-c) and F (d-f) k -points for various values of U_{eff} . The KS orbitals are represented by a gray 0.02 e/bohr^3 isosurface. We plot the charge density from the KS orbitals in a $(11\bar{2})$ plane, with colour saturation levels indicated by the colour bar.

Stroppa and Picozzi [13]. An experimental study comparing VB_{max} energies of BFO, Bi_2O_3 and Fe_2O_3 also proposes a non-negligible contribution from the Bi s states, as well as Fe d states, to the VB_{max} of BFO [57]. The findings of these two previous works are better reflected in our calculated electronic structures of the VB_{max} for $U_{\text{eff}} \geq 2 \text{ eV}$.

From the projected conduction bands (Fig. 5), we see little change in the *elemental* contributions to the CB_{min} ; Fe dominates the CB_{min} for all U_{eff} investigated here. The band structures do indicate, however, a change in the relative *orbital* contributions to the CB_{min} . We might expect the three lowest unoccupied bands to be Fe t_{2g} in character and the two next unoccupied bands to be Fe e_g , based on the octahedrally coordinated Fe. Indeed, we see at the Γ -point that the five Fe d bands form neatly into distinct triply and doubly degenerate sets. Detailed analysis of the crystal-field splitting in this system could be achieved using Wannier functions as in Ref. [58], though this lies beyond the scope of the present work. The designation of the five green (Fe) bands into t_{2g} and e_g groups in order of increasing energy is supported by the projected DOS, in which we see the energy difference between the e_g and t_{2g} manifolds decrease with an increase in U_{eff} . For values of U_{eff} greater than 4 eV however, Fig. 5 suggests that one of the two Fe e_g bands dips below the three Fe t_{2g} bands. That is, above a U_{eff} of 4 eV, the character of the CB_{min} transitions from Fe t_{2g} to Fe e_g .

To investigate the shift in orbital character from t_{2g} to e_g further, we plot the lowest unoccupied Kohn-Sham (KS) orbitals in Fig. 6. Because the CB_{min} is located at $Z = [0.5, 0.5, 0.5]$ for $U_{\text{eff}} \leq 4 \text{ eV}$ and at $F = [0.5, 0.5, 0.0]$ for $U_{\text{eff}} > 4 \text{ eV}$, we plot

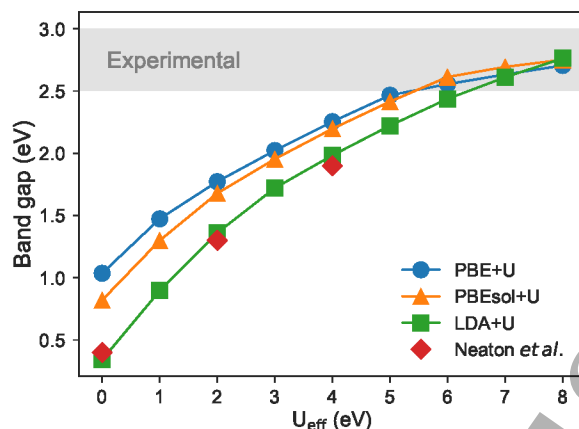


Figure 7. Variation in calculated electronic band gap as a function of U_{eff} for the PBE+U (blue circles), PBEsol+U (orange triangles) and LDA+U (green squares) xc functionals. The range of band gaps reported in the experimental literature is shown as the shaded region. The LDA+U results reported by Neaton *et al.* [25] are shown for comparison.

the KS orbitals at each of these locations, for relevant values of U_{eff} . To visualise some of the more subtle changes, we plot the charge density from the KS orbitals in a $(11\bar{2})$ plane, in addition to the isosurface. These plots highlight two distinct effects that U_{eff} has on the character of the CB_{min} .

Firstly, at the Z point (which is the CB_{min} for $U_{\text{eff}} < 5$ eV), there is a gradual increase in hybridisation between the Fe t_{2g} and Bi p orbitals along the $[111]_{pc}$ direction as U_{eff} increases, evident from the increase in intensity between Fe and Bi on the $(11\bar{2})$ plane. This increase in overlap between Fe and Bi states contributes to the decrease in m_e^* between a U_{eff} of 0 and 4 eV.

Secondly, at the F point, we see a transition from t_{2g} to e_g character from the KS isosurface plot as U_{eff} increases from 3 eV to 5 eV, as expected from the band structures. Additionally we see a slight increase in intensity around the Bi and O atoms on the $(11\bar{2})$ plane. The transition to e_g character is associated with a further decrease in m_e^* , possibly due to the increased overlap with O p states. Above 5 eV there is little change in the KS orbitals (see Fig. S3 of the SI [47]), and correspondingly, we see little change in m_e^* .

The significant shift in the location and character of the CB_{min} for $U_{\text{eff}} > 4$ eV suggests that $U_{\text{eff}} = 4$ eV be taken as a maximum, at least in cases for which the character and curvature of the CB_{min} plays a significant role.

Given that U_{eff} is sometimes chosen such that the calculated band gap matches that found in experiment, we now explicitly examine the effect of U_{eff} on the electronic band gap. We expect that, as U_{eff} increases, the band gap will increase due to the enhanced localisation of the Fe d orbitals. Indeed we see such a relationship in Fig. 7, where we plot the electronic band gap against U_{eff} . The trends across the PBE+U, PBEsol+U and LDA+U functionals are similar, though the LDA+U gaps are significantly smaller

than those of the PBE+U and PBEsol+U functionals for all $U_{\text{eff}} \leq 6$ eV. The LDA+U values are in excellent agreement with those found in Ref. [25], also plotted in Fig. 7. In Ref. [28], the PBE+U band gap is calculated from the theoretical optical absorption spectrum to be 2.58 eV for a U_{eff} of 5 eV. Their band gap value is 0.11 eV higher than the electronic band gap found in this work, 2.47 eV, for the same U_{eff} value.

In order to match the experimental band gap range of 2.5–3.0 eV [59, 60, 61], a U_{eff} of 5 eV or larger is clearly required. As we have seen above however, the ordering of the Fe d orbitals at the CB_{min} inverts for $U_{\text{eff}} > 4$ eV, suggesting that fitting U_{eff} to the electronic band gap alone may introduce some spurious effects. While a $U_{\text{eff}} < 4$ eV underestimates the electronic band gap, we note that the DFT+U method can, at best, only correct the self-interaction error in the orbitals to which it is applied (in this case the Fe d orbitals). Self-interaction error from the other BFO orbitals, together with other sources of error intrinsic to Kohn-Sham DFT [62] are not accounted for by using DFT+U. That is to say, we ought to expect some remaining underestimation of the electronic band gap, even for the value of U_{eff} that most accurately localises the Fe d orbitals.

4. Conclusions

We have employed the DFT+U method to calculate the optimum crystal geometry and electronic structure of the $R3c$ phase of BFO for a range of U_{eff} between 0 and 8 eV, applied to the Fe d orbitals. We showed that the Bi displacement from its centrosymmetric position, the rotation of the FeO_6 octahedra, the distortion of the octahedra, and the spontaneous polarisation change negligibly within the U_{eff} range typically employed in the context of BFO.

The electronic structure, in contrast, varies significantly with U_{eff} , as designed: the application of U_{eff} is meant to correct the over-delocalisation of the states to which it is applied. With increasing U_{eff} , we find that the character of the states near the band edges changes, in addition to the band gap, leading to enormous changes in calculated charge carrier effective masses. In particular, the ordering of the Fe d orbitals at the CB_{min} inverts for U_{eff} values larger than 4 eV.

Using a U_{eff} of 4 eV leads to a 10–25% underestimation in the calculated band gap with respect to experimental values. To match the experimental band gap, a U_{eff} value of between 5 and 8 eV would be required. However, in this range of U_{eff} , the CB_{min} is Fe e_g in character rather than the Fe t_{2g} character found for U_{eff} values less than 5 eV. The widespread practice of selecting the U_{eff} parameter to match the experimental band gap therefore clearly needs to be exercised with caution, particularly in cases for which the character of the band edges play a significant role. We strongly recommend a thorough analysis of the effect of U_{eff} on the calculated electronic structure before proceeding with calculations that depend on the character of the band edges such as charge carrier effective masses, optical absorption energies and oxidation energies.

5. Acknowledgements

The authors acknowledge the use of the UCL Legion (Legion@UCL) and Grace (Grace@UCL) High Performance Computing Facilities, and associated support services, in the completion of this work.

6. Bibliography

- [1] Lee J H, Fina I, Marti X, Kim Y H, Hesse D and Alexe M 2014 *Advanced Materials* **26** 7078–7082 ISSN 15214095 URL <http://doi.wiley.com/10.1002/adma.201402558>
- [2] Ji W, Yao K and Liang Y C 2010 *Advanced Materials* **22** 1763–1766 ISSN 09359648 URL <http://doi.wiley.com/10.1002/adma.200902985>
- [3] Paillard C, Bai X, Infante I C, Guennou M, Geneste G, Alexe M, Kreisel J and Dkhil B 2016 Photovoltaics with Ferroelectrics: Current Status and Beyond URL <http://doi.wiley.com/10.1002/adma.201505215>
- [4] Shvartsman V V, Kleemann W, Haumont R and Kreisel J 2007 *Applied Physics Letters* **90** 172115 ISSN 00036951 URL <http://scitation.aip.org/content/aip/journal/apl/90/17/10.1063/1.2731312>
- [5] Lebeugle D, Colson D, Forget A and Viret M 2007 *Applied Physics Letters* **91** 022907 ISSN 00036951 URL <http://scitation.aip.org/content/aip/journal/apl/91/2/10.1063/1.2753390>
- [6] Fridkin V M 2001 *Crystallography Reports* **46** 654–658 ISSN 1063-7745 URL <http://link.springer.com/10.1134/1.1387133>
- [7] Ji W, Yao K and Liang Y C 2011 *Physical Review B* **84** 094115 ISSN 1098-0121 URL <https://link.aps.org/doi/10.1103/PhysRevB.84.094115>
- [8] Yang S Y, Seidel J, Byrnes S J, Shafer P, Yang C H, Rossell M D, Yu P, Chu Y H, Scott J F, Ager J W, Martin L W and Ramesh R 2010 *Nature nanotechnology* **5** 143–7 ISSN 1748-3395 URL <http://www.ncbi.nlm.nih.gov/pubmed/20062051>
- [9] Seidel J, Martin L W, He Q, Zhan Q, Chu Y H, Rother A, Hawkridge M E, Maksymovych P, Yu P, Gajek M, Balke N, Kalinin S V, Gemming S, Wang F, Catalan G, Scott J F, Spaldin N A, Orenstein J and Ramesh R 2009 *Nature materials* **8** 229–34 ISSN 1476-1122 URL <http://dx.doi.org/10.1038/nmat2373>
- [10] Sando D, Barthélémy A and Bibes M 2014 *Journal of Physics: Condensed Matter* **26** 473201 ISSN 0953-8984 URL <https://doi.org/10.1088/0953-8984/26/47/473201>
- [11] Sando D, Xu B, Bellaiche L and Nagarajan V 2016 *Applied Physics Reviews* **3** 011106 ISSN 19319401 (*Preprint* 1512.05835) URL <http://scitation.aip.org/content/aip/journal/apr/2/3/1/10.1063/1.4944558>
- [12] Ederer C and Spaldin N 2005 *Physical Review B* **71** 060401 ISSN 1098-0121 URL <http://link.aps.org/doi/10.1103/PhysRevB.71.060401>
- [13] Stroppa A and Picozzi S 2010 *Physical Chemistry Chemical Physics* **12** 5405–16 ISSN 1463-9084 URL <http://www.ncbi.nlm.nih.gov/pubmed/20445921>
- [14] Bhatnagar A, Roy Chaudhuri A, Heon Kim Y, Hesse D and Alexe M 2013 *Nature Communications* **4** 2835 ISSN 2041-1723 URL <http://www.nature.com/doi/10.1038/ncomms3835>
- [15] Rong Q Y, Wang L L, Xiao W Z and Xu L 2015 *Physica B: Condensed Matter* **457** 1–4 ISSN 09214526 URL <http://linkinghub.elsevier.com/retrieve/pii/S0921452614006942>
- [16] Wang Q, Tan Q and Liu Y 2015 *Computational Materials Science* **105** 1–5 ISSN 09270256 URL <http://linkinghub.elsevier.com/retrieve/pii/S0927025615002499>
- [17] Rondinelli J M, May S J and Freeland J W 2012 *MRS Bulletin* **37** 261–270 ISSN 0883-7694 URL http://www.journals.cambridge.org/abstract_S0883769412000498
- [18] Borisevich A Y, Chang H J, Huijben M, Oxley M P, Okamoto S, Niranjana M K, Burton J D,

- Tsymbal E Y, Chu Y H, Yu P, Ramesh R, Kalinin S V and Pennycook S J 2010 *Physical Review Letters* **105** 087204 ISSN 0031-9007 URL <http://link.aps.org/doi/10.1103/PhysRevLett.105.087204>
- [19] Zhou C C, Jin K x, Luo B C, Cao X s and Chen C L 2010 *Materials Letters* **64** 1713–1716 ISSN 0167577X URL <http://linkinghub.elsevier.com/retrieve/pii/S0167577X10003551>
- [20] Yu P, Luo W, Yi D, Zhang J X, Rossell M D, Yang C H, You L, Singh-Bhalla G, Yang S Y, He Q, Ramasse Q M, Erni R, Martin L W, Chu Y H, Pantelides S T, Pennycook S J and Ramesh R 2012 *Proceedings of the National Academy of Sciences of the United States of America* **109** 9710–5 ISSN 1091-6490 URL <http://www.pnas.org/content/109/25/9710>
- [21] Kim Y M, Kumar A, Hatt A, Morozovska A N, Tselev A, Biegalski M D, Ivanov I, Eliseev E A, Pennycook S J, Rondinelli J M, Kalinin S V and Borisevich A Y 2013 *Advanced Materials* **25** 2497–2504 ISSN 09359648 URL <http://doi.wiley.com/10.1002/adma.201204584>
- [22] Dudarev S L, Savrasov S Y, Humphreys C J, Sutton A P, Botton G A, Savrasov S Y, Humphreys C J and Sutton A P 1998 *Physical Review B* **57** 1505–1509 ISSN 1098-0121 URL <http://link.aps.org/doi/10.1103/PhysRevB.57.1505>
- [23] Pavarini E, Koch E, Anders F and Jarrell M E 2012 *Correlated Electrons: From Models to Materials (Schriften des Forschungszentrums Jülich. Reihe Modeling and simulation vol 2)* (Jülich: Forschungszentrum Jülich GmbH) ISBN 9783893367962 URL <http://hdl.handle.net/2128/4611>
- [24] Wang L, Maxisch T and Ceder G 2006 *Physical Review B* **73** 195107 ISSN 1098-0121 (*Preprint* 9605103) URL <http://link.aps.org/doi/10.1103/PhysRevB.73.195107>
- [25] Neaton J B, Ederer C, Waghmare U V, Spaldin N A and Rabe K M 2005 *Physical Review B* **71** 014113 ISSN 1098-0121 URL <http://link.aps.org/doi/10.1103/PhysRevB.71.014113>
- [26] Cococcioni M and de Gironcoli S 2005 *Physical Review B* **71** 035105 ISSN 1098-0121 (*Preprint* 0405160) URL <http://link.aps.org/doi/10.1103/PhysRevB.71.035105>
- [27] Kornev I A, Lisenkov S, Haumont R, Dkhil B and Bellaiche L 2007 *Physical Review Letters* **99** 227602 ISSN 0031-9007 URL <http://link.aps.org/doi/10.1103/PhysRevLett.99.227602>
- [28] Young S M, Zheng F and Rappe A M 2012 *Physical Review Letters* **109** 236601 ISSN 0031-9007 URL <http://link.aps.org/doi/10.1103/PhysRevLett.109.236601>
- [29] Shenton J K, Cheah W L and Bowler D R Manuscript in preparation
- [30] Kresse G and Hafner J 1993 *Physical Review B* **47** 558–561 ISSN 01631829 (*Preprint* 0927-0256(96)00008) URL <https://link.aps.org/doi/10.1103/PhysRevB.47.558>
- [31] Kresse G and Hafner J 1994 *Physical Review B* **49** 14251–14269 ISSN 01631829 URL <https://link.aps.org/doi/10.1103/PhysRevB.49.14251>
- [32] Kresse G and Furthmüller J 1996 *Computational Materials Science* **6** 15–50 ISSN 09270256 (*Preprint* 0927-0256(96)00008) URL <http://linkinghub.elsevier.com/retrieve/pii/S0927025696000080>
- [33] Kresse G and Furthmüller J 1996 *Physical Review B* **54** 11169–11186 ISSN 0163-1829 (*Preprint* 0927-0256(96)00008) URL <http://link.aps.org/doi/10.1103/PhysRevB.54.11169>
- [34] Blöchl P E 1994 *Physical Review B* **50** 17953–17979 ISSN 01631829 (*Preprint* arXiv:1408.4701v2) URL <https://link.aps.org/doi/10.1103/PhysRevB.50.17953>
- [35] Kresse G and Joubert D 1999 *Physical Review B* **59** 1758–1775 ISSN 0163-1829 URL <https://link.aps.org/doi/10.1103/PhysRevB.59.1758>
- [36] Monkhorst H J and Pack J D 1976 *Physical Review B* **13** 5188–5192 ISSN 0556-2805 URL <http://link.aps.org/doi/10.1103/PhysRevB.13.5188>
- [37] Perdew J P, Burke K and Ernzerhof M 1996 *Physical Review Letters* **77** 3865–3868 ISSN 0031-9007 URL <http://link.aps.org/doi/10.1103/PhysRevLett.77.3865>
- [38] Perdew J P, Ruzsinszky A, Csonka G I, Vydrov O A, Scuseria G E, Constantin L A, Zhou X and Burke K 2008 *Physical Review Letters* **100** 136406 ISSN 0031-9007 (*Preprint* 0707.2088) URL <https://link.aps.org/doi/10.1103/PhysRevLett.100.136406><http://link.aps.org/doi/10.1103/PhysRevLett.100.136406>

- [39] Palewicz A, Przeniosło R, Sosnowska I and Hewat A W 2007 *Acta Crystallographica Section B Structural Science* **63** 537–544 ISSN 0108-7681 URL <http://scripts.iucr.org/cgi-bin/paper?ck5024>
- [40] Sosnowska I, Neumaier T P and Steichele E 1982 *Journal of Physics C: Solid State Physics* **15** 4835–4846 ISSN 0022-3719 URL <https://doi.org/10.1088/0022-3719/15/23/020>
- [41] King-Smith R D and Vanderbilt D 1993 *Physical Review B* **47** 1651–1654 ISSN 0163-1829 URL <http://link.aps.org/doi/10.1103/PhysRevB.47.1651>
- [42] Vanderbilt D and King-Smith R D 1993 *Physical Review B* **48** 4442–4455 ISSN 0163-1829 URL <http://link.aps.org/doi/10.1103/PhysRevB.48.4442>
- [43] Resta R 1994 *Ferroelectrics* **151** 49–58 ISSN 0015-0193 URL <http://link.aps.org/doi/10.1103/RevModPhys.66.899>
- [44] Fonari A and Sutton C 2012 Effective Mass Calculator URL <https://github.com/afonari/emc>
- [45] Hautier G, Miglio A, Ceder G, Rignanese G M and Gonze X 2013 *Nature Communications* **4** ISSN 2041-1723 URL <http://www.nature.com/doifinder/10.1038/ncomms3292>
- [46] Hautier G, Miglio A, Waroquiers D, Rignanese G M and Gonze X 2014 *Chemistry of Materials* **26** 5447–5458 ISSN 0897-4756 URL <http://pubs.acs.org/doi/abs/10.1021/cm404079a>
- [47] Shenton J K, Cheah W L and Bowler D R 2017 Supplementary information for a study of DFT+U in the context of BiFeO₃ URL <https://doi.org/10.5281/zenodo.841395>
- [48] Glazer A M 1972 *Acta Crystallographica Section B Structural Crystallography and Crystal Chemistry* **28** 3384–3392 ISSN 05677408 URL <http://scripts.iucr.org/cgi-bin/paper?S0567740872007976>
- [49] Catalan G and Scott J F 2009 *Advanced Materials* **21** 2463–2485 ISSN 09359648 URL <http://doi.wiley.com/10.1002/adma.200802849>
- [50] Moreau J, Michel C, Gerson R and James W 1971 *Journal of Physics and Chemistry of Solids* **32** 1315–1320 ISSN 00223697 URL <http://linkinghub.elsevier.com/retrieve/pii/S0022369771801890>
- [51] Kubel F and Schmid H 1990 *Acta Crystallographica Section B* **46** 698–702 ISSN 16005740 URL <http://scripts.iucr.org/cgi-bin/paper?S0108768190006887>
- [52] Megaw H D and Darlington C N W 1975 *Acta Crystallographica Section A* **31** 161–173 ISSN 0567-7394 URL <http://scripts.iucr.org/cgi-bin/paper?S0567739475000332>
- [53] Chen Z, Prosandeev S, Luo Z L, Ren W, Qi Y, Huang C W, You L, Gao C, Kornev I A, Wu T, Wang J, Yang P, Sritharan T, Bellaiche L and Chen L 2011 *Physical Review B* **84** 094116 ISSN 1098-0121 URL <http://link.aps.org/doi/10.1103/PhysRevB.84.094116>
- [54] Chu S, Singh D, Wang J, Li E P and Ong K 2012 *Laser & Photonics Reviews* **6** 684–689 ISSN 18638880 URL <http://doi.wiley.com/10.1002/lpor.201280022>
- [55] Tütüncü H M and Srivastava G P 2008 *Physical Review B* **78** 235209 ISSN 1098-0121 URL <http://link.aps.org/doi/10.1103/PhysRevB.78.235209>
- [56] Jin Y, Lu X, Zhang J, Kan Y, Bo H, Huang F, Xu T, Du Y, Xiao S and Zhu J 2015 *Scientific Reports* **5** 12237 ISSN 2045-2322 URL <http://www.nature.com/articles/srep12237>
- [57] Li S, Morasch J, Klein A, Chirila C, Pintilie L, Jia L, Ellmer K, Naderer M, Reichmann K, Gröting M and Albe K 2013 *Physical Review B* **88** 045428 ISSN 1098-0121 URL <https://link.aps.org/doi/10.1103/PhysRevB.88.045428>
- [58] Scaramucci A, Ammann J, Spaldin N A and Ederer C 2015 *Journal of Physics: Condensed Matter* **27** 175503 ISSN 0953-8984 URL <http://stacks.iop.org/0953-8984/27/i=17/a=175503%0A>
- [59] Gao F, Yuan Y, Wang K F, Chen X Y, Chen F, Liu J M and Ren Z F 2006 *Applied Physics Letters* **89** 102506 ISSN 00036951 URL <http://scitation.aip.org/content/aip/journal/apl/89/10/10.1063/1.2345825>
- [60] Kumar A, Rai R C, Podraza N J, Denev S, Ramirez M, Chu Y H, Martin L W, Ihlefeld J, Heeg T, Schubert J, Schlom D G, Orenstein J, Ramesh R, Collins R W, Musfeldt J L and Gopalan V 2008 *Applied Physics Letters* **92** 121915 ISSN 00036951 URL <http://scitation.aip.org/content/aip/journal/apl/92/12/10.1063/1.2901168>

- 1
2
3
4
5 [61] Moubah R, Schmerber G, Rousseau O, Colson D and Viret M 2012 *Applied Physics Express* **5**
6 035802 ISSN 1882-0778 URL <http://stacks.iop.org/1882-0786/5/035802>
7 [62] Perdew J P 1986 *International Journal of Quantum Chemistry* **30** 451–451 ISSN 0020-7608 URL
8 <http://doi.wiley.com/10.1002/qua.560300314>
9
10
11
12
13
14
15
16
17
18
19
20
21
22
23
24
25
26
27
28
29
30
31
32
33
34
35
36
37
38
39
40
41
42
43
44
45
46
47
48
49
50
51
52
53
54
55
56
57
58
59
60

Accepted Manuscript